REACTION ENGINEERING, KINETICS AND CATALYSIS

AIChE Journal

DOI10.1002/aic.16692

Continuous and complete conversion of high concentration *p*-nitrophenol in a flow-through membrane reactor

Jianfeng Miao, Jia Lu, Hong Jiang, Yefei Liu and Weihong Xing

State Key Laboratory of Materials-Oriented Chemical Engineering, Nanjing Tech University, Nanjing 210009, P.R. China

Xuebin Ke*

School of Engineering and Computer Science, University of Hull, HU6 7RX, United Kingdom

Rizhi Chen*

State Key Laboratory of Materials-Oriented Chemical Engineering, Nanjing Tech University, Nanjing 210009, P.R. China

*Corresponding author. X.Ke@hull.ac.uk; rizhichen@njtech.edu.cn

Accepted Article

This is the peer reviewed version of the following article: Miao, J, Lu, J, Jiang, H, et al. Continuous and complete conversion of high concentration p-nitrophenol in a flow-through membrane reactor. AIChE J. 2019;e16692, which has been published in final form at https://doi.org/10.1002/aic.16692. This article may be used for non-commercial purposes in accordance With Wiley Terms and Conditions for self-archiving.

This article has been accepted for publication and undergone full peer review but has not been through the copyediting, typesetting, pagination and proofreading process which may lead to differences between this version and the Version of Record. Please cite this article as doi: 10.1002/aic.16692

© 2019 American Institute of Chemical Engineers

Received: Jan 14, 2019;Revised: May 23, 2019;Accepted: Jun 04, 2019

This article is protected by copyright. All rights reserved.

Accepted Article

Abstract

Here, we report on a green and effective method for the continuous and complete conversion of high concentrations of *p*-nitrophenol (PNP) using a flow-through membrane reactor and less $NaBH_4$. The catalytic membrane was successfully fabricated by loading Pd nanoparticles onto the surface of a branched TiO_2 nanorod-functionalized ceramic membrane. The modification with branched TiO_2 nanorods can significantly improve the loading amount of Pd nanoparticles onto ceramic membranes, resulting in enhanced catalytic performance. With 6 mg of Pd, 93 $L \cdot m^{-2} \cdot h^{-1}$ of flux density and 8.04 cm^2 of membrane surface area in the flow-through membrane reactor, PNP at a concentration of 4000 ppm can be converted to high-value p-aminophenol using less $NaBH_4$ (using a molar ratio of $NaBH_4$:PNP of 9.6) within 24 seconds at 30 ^oC. More importantly, the conversion can be continuously and stably performed for 240 minutes.

Keywords: *p*-Nitrophenol, continuous and complete conversion, Pd nanoparticles, branched TiO_2 nanorods, flow-through membrane reactor

This article is protected by copyright. All rights reserved.

Accepted Article

Introduction

p-Nitrophenol (PNP) is a common environmental pollutant in water and is therefore a great public concern.[1] It is usually used as a precursor or a synthetic intermediate in the industrial manufacturing of analgesics, pharmaceuticals, insecticides, dyes and other chemicals.[2-4] PNP may bring about significant health hazards because of its carcinogenic toxicity. Short-term inhalation or ingestion in humans can cause headaches, drowsiness, nausea and cyanosis, even at low concentrations.[5,6] The concentration of PNP in industrial wastewater is usually much higher than 500 mg/L.[7] Therefore, the complete elimination of this compound from industrial effluents is a matter of concern for environmental protection. Various methods have been proposed for the treatment of PNP-contaminated wastewater.[8] The conventional physical methods (sedimentation, filtration, adsorption, etc.) transfer the contaminants into other forms and cannot solve the waste disposal problem.[9] Biological methods may require long treatment time, and complete degradation may be impossible,

This article is protected by copyright. All rights reserved.

especially for effluents containing PNP at a high concentration.[10-12] Thus, the development of effective chemical methods to convert PNP to high-value products or to achieve complete degradation is urgently needed.

Catalytic reduction of PNP to *p*-aminophenol, an important chemical intermediate, is a feasible method for turning waste into a renewable resource.[13,14] In addition, aromatic amines are less toxic and considerably easier to mineralize than their corresponding nitroaromatics.[15,16] Conventional metal-acid reduction methods employ reagents such as iron-acids or tin-acids. The major disadvantage of such reduction processes is the generation of large amounts of metal oxide sludge that is associated with severe pollution problems.[17] One-step hydrogenation of PNP in the presence of metal catalysts or supported metal catalysts is considered to be the most promising process because of its high efficiency and environmentally friendly properties.[18] As a strong reducing agent, $NaBH_4$ can effectively reduce PNP to *p*-aminophenol under mild operation conditions (room temperature and atmospheric pressure).[19] Thus, the direct reduction of PNP with $NaBH_4$ as a reducing agent is considered to be an efficient and greener catalytic route for the conversion of PNP.

In the practical treatment of industrial wastewater, fixed-bed reactors and slurry reactors inevitably develop problems. For a fixed-bed reactor, fine catalysts cannot be directly used, and their inner surface cannot be fully utilized. In addition, the regeneration and replacement of catalysts are inconvenient. In a slurry reactor, metal nanoparticles that are present on the

Accepted Article

This article is protected by copyright. All rights reserved.

Accepted Article

powdered catalysts easily aggregate or leak, and it is difficult to separate them from the reaction system.[20] Catalytic membranes exhibit good particle distribution, and no additional separation is required.[21,22] Moreover, the porous membrane structure and flow-through mode can enhance the catalytic efficiency by increasing mass transfer.[23] These advantages allow flow-through catalytic membrane reactors to efficiently treat industrial wastewaters that contain high concentrations of PNP. Wang et al.[24] developed a novel poly (vinylidene fluoride) membrane with Pd/poly (methacrylic acid) microspheres immobilized inside the membrane pores. Its use in the catalytic reduction of PNP indicated that a conversion of 99.8% could be achieved in a cross-flow model. Domènech et al.[25] reported on the synthesis of Pd nanoparticles in sulfonated polyethersulfone membranes. The catalytic performance was evaluated by following the reduction of PNP in the presence of $NaBH_4$. Greater than 90% of the PNP was reduced within 4 hours using a single reaction step, and deactivation was observed after consecutive catalytic cycles. Our group[26] successfully demonstrated that the use of TiO_2 nanorod-functionalized ceramic membranes is an effective approach for enhancing the loading amount of Pd and the corresponding catalytic activity. However, the catalytic membranes obtained when used directly in a batch reactor could not achieve continuous conversion of PNP. Furthermore, although complete conversion of PNP can be achieved, a high molar ratio of $NaBH_4$ to PNP like 100 is required.[27,28] An excess of the reductant $NaBH_4$ will increase the treatment cost significantly. Therefore, the efficient

This article is protected by copyright. All rights reserved.

transformation of PNP remains a great challenge.

The objective of this work was to accomplish the continuous and complete conversion of high concentrations of PNP by using less $NaBH_4$. We designed a flow-through catalytic membrane reactor for use in a continuous mode. Furthermore, branched rutile TiO_2 nanorod arrays were synthesized on an alumina ceramic membrane using a simple hydrothermal grafting method. Pd nanoparticles were then immobilized on the surface of the modified ceramic membranes by a sol impregnation method (denoted as Pd/BTiO_2-CM). For comparison, Pd nanoparticles loaded onto bare ceramic membranes (Pd/CM), and TiO_2 nanorod array-modified ceramic membranes (Pd/TiO_2-CM) were also fabricated using the same conditions. The crystallinity, morphology and structures of the prepared catalytic membranes were investigated to understand the dependence of catalytic performance on their microstructure.

Experimental

Preparation of catalytic membranes

Synthesis of TiO_2 nanorods and branched TiO_2 nanorods on ceramic membranes

TiO_2 nanorod arrays on sheet Al_2O_3 ceramic membranes (circular, 3.2 cm in diameter, 1.6 mm in thickness and 30% in porosity) were obtained via the following two-step hydrothermal method.[26] Twenty mL of concentrated hydrochloric acid (Analytical Reagent,

Accepted Article

This article is protected by copyright. All rights reserved.

Accepted Article

mass fraction 36.5-38%) were mixed with 20 mL of deionized water. After stirring at 30 °C for 10 min, 955 μL of titanium butoxide (Chemically Pure, 98.0%) were added to the mixture. The feedstock prepared above was injected into a Teflon-lined stainless steel autoclave in which a piece of ceramic membrane was placed vertically. Hydrothermal synthesis was initiated when the autoclave was placed in an electric oven and maintained at 150°C for 5 hours. In the second hydrothermal synthesis process, similarly to the first step, 3 mL of a saturated NaCl aqueous solution were added to the same mixture as described above and the hydrothermal synthesis was conducted at 150 °C for 20 hours. Chloride ions can accelerate the growth of TiO_2 in the direction of the top (001) crystal facet.[29] Thus, TiO_2 nanorods having a greater length to diameter ratio can be synthesized by the introduction of NaCl.

Branched TiO_2 nanorod arrays were grown by immersing the TiO_2 nanorod-modified ceramic membranes prepared above in an autoclave filled with 40 mL of deionized water, 0.1 mL of hydrochloric acid and 0.8 mL of a titanium chloride solution (Analytical Reagent, mass fraction 15-20%). The autoclave was then sealed and maintained at a constant temperature of 80 °C for 16 hours. Finally, to eliminate the influence of the chloride impurity, the obtained sample was rinsed extensively with deionized water until it was neutral, and dried at 60 °C for 4 hours.

The branched TiO_2 nanorod-modified ceramic membranes were further modified with N-(β-aminoethyl)-γ-aminopropyl trimethoxy silane (AAPTS) by immersing them in 50 mL of

This article is protected by copyright. All rights reserved.

an AAPTS dichloromethane solution (0.1 g/L) at 25 °C for 8 hours. The prepared sample was designated as $BTiO_2$-CM-AAPTS.

Synthesis of catalytic membranes

Three catalytic membranes (Pd/CM, Pd/TiO_2-CM and Pd/$BTiO_2$-CM) were prepared by a sol impregnation method.[30] Typically, 0.56 g of palladium acetate (mass fraction of Pd is approximately 47%) and 5.55 g of polyvinylpyrrolidone (PVP, K30, Guaranteed Reagent) were dissolved in 50 mL of ethanol (Analytical Reagent, 99.7%), and the mixture was then stirred at 60 °C for 2 hours to prepare the Pd nanoparticle colloid. The bare ceramic membranes, the TiO_2 nanorod-modified ceramic membranes and the branched TiO_2 nanorod-modified ceramic membranes were immersed in the Pd nanoparticle colloid (50 mL, 0.05 mol/L) at 40 °C for 12 hours. The samples were washed with ethanol to remove the Pd nanoparticles that were not firmly loaded onto the ceramic membranes and/or TiO_2 nanorods, and then dried at ambient temperature.

Characterization of Catalytic Membranes

Structure and morphology of catalytic membranes

The crystal structure of the catalytic membranes was determined by X-ray diffraction (XRD, Miniflex-600) analysis at a scan rate of 10° per min in the range of 5-70°. The surface morphology of the catalytic membranes was characterized using a field emission scanning electron microscope (FESEM, Hitachi S-4800II). The Brunauer-Emmett-Teller (BET) surface

Accepted Article

This article is protected by copyright. All rights reserved.

area of the catalytic membranes was measured by N_2 physisorption using a physical adsorption apparatus (Micromeritics, ASAP 2020). The pore size of the catalytic membranes was determined using a mercury intrusion porosimeter (Poremaster GT-60).

Pd nanoparticles in catalytic membranes

The distribution of elemental Pd in the catalytic membranes was determined by energy-dispersive X-ray spectroscopy (EDS, Horiba Emax). Inductively coupled plasma emission spectroscopy (ICP, Optima 2000 DV) was used to evaluate the Pd content. The solutions for ICP analyses were obtained by immersing the samples in 20 mL of an aqueous solution of 10% (v/v) nitric acid (65-68%) at 60 °C for 2 hours. X-ray photoelectron spectrometry (XPS, Thermo ESCALAB 250) was conducted to analyze the valence state of the Pd in the catalytic membrane. Powders (0.1 g) were scraped off the surface of the catalytic membrane and were subjected to XPS analysis. Particle size and distribution of Pd were investigated by high-resolution transmission electron microscopy (HRTEM, JEM-2010). In this study, the prepared catalytic membrane was a circular flat membrane with a diameter of 3.2 cm. For TEM tests, 0.05 g of powders were scraped off the surface of the catalytic membrane and dispersed in 10 mL of ethanol. To obtain reproducible results, the particle size of the Pd was evaluated by counting more than 100 particles and samples were tested in triplicate.

Determination of pure water flux

Accepted Article

This article is protected by copyright. All rights reserved.

Accepted Article

Pure water permeation by the membranes was investigated using a dead-end permeation apparatus at a transmembrane pressure of 0.2 bar and a temperature of 18 ^{o}C. The effective diameter of the membrane in contact with the solution was 2.6 cm. The pure water flux through the catalytic membrane was calculated using the following equation:

$$F = \frac{Q}{A * t * \mathrm{P}}$$

where F is the pure water flux through the catalytic membrane ($L \cdot m^{-2} \cdot h^{-1} \cdot bar^{-1}$), Q is the volume of penetration liquid (L), A is the effective membrane area (m^2), t is the permeation time (h) and P is the transmembrane pressure (bar).

Evaluation of Catalytic Performance

Reduction of PNP was performed in a flow-through membrane reactor system in two modes (cycle mode and continuous mode). The surface area of the catalytic membrane in contact with the reactant solution was 8.04 cm^2 and the thickness of the catalytic membrane was 0.16 cm. As shown in Figure 1, in the former mode, 60 mL of reaction solution (10 mL of analytically pure ethanol and 50 mL of deionized water) containing a mixture of $NaBH_4$ (0.65 g) and PNP (0.25 g) at a molar ratio of 9.6 was introduced into the storage tank. The molar ratios of PNP to Pd were 174 (Pd/CM), 128 (Pd/TiO_2-CM) and 64 (Pd/BTiO_2-CM). The reaction solution was passed through the pores of the catalytic membrane with the assistance of a peristaltic pump at a flow rate of 45 mL/min and then allowed to flow to a storage tank. The reaction was initiated when the reaction solution flowed into the membrane

This article is protected by copyright. All rights reserved.

module and conversion of the PNP occurred within 60 minutes, which defined the reaction time. A water bath was used to maintain the reaction temperature at 30 °C, and the reactor was operated under a pressure of 0.25 bar. Samples of the reaction mixture were taken from the sampling port in intervals of 5 minutes and were analyzed by high-performance liquid chromatography (HPLC, Agilent 1200 series). The initial reaction rate ($mmol \cdot L^{-1} \cdot min^{-1}$) was defined as the amount of PNP consumed per minute during the first 5 minutes. In the continuous mode, the reaction solution containing the same concentration of PNP and $NaBH_4$ flowed continuously through the membrane module. The flow rate of the reaction mixture through the reactor system was controlled by the peristaltic pump. Furthermore, in order to improve the catalytic efficiency, two membrane modules were connected in series. The reaction temperature was maintained at 30 °C and the reaction pressure was 0.05 bar. The permeate from the first membrane was tested by ICP to investigate whether there was Pd in the permeate between the two catalytic membranes. The products were further analyzed by gas chromatography- mass spectrometry (GC-MS, GC-2014). Ten mL of products were extracted with 10 mL of diethyl ether at 30 ^{o}C for 2 hours, and the organic phase was used for GC-MS analysis. The total residence time of the reaction solution in the two successive catalytic membranes is defined as:

$$\text{residence time (s)} = \frac{\text{pore volume of membranes } (cm^3)}{\text{volumetric flow rate of reaction solution } (cm^3/s)}$$

Accepted Article

This article is protected by copyright. All rights reserved.

Accepted Article

Results and Discussion

Characterization of catalytic membranes

Structure and morphology of catalytic membranes

As illustrated in Figure 2, the diffraction lines of Pd/TiO_2-CM and Pd/BTiO_2-CM show similar patterns. With the exception of the diffraction peaks from the Al_2O_3 ceramic membrane, there are four featured peaks at 27.4°, 36.2°, 41.2° and 54.3° which can be indexed as the (110), (101), (111) and (211) planes of rutile phase TiO_2 (JCPDS No. 21-1276).[31] This indicates that TiO_2 nanorods and branches all consist of pure rutile phase TiO_2. However, compared to Pd/TiO_2-CM, the diffraction peaks of TiO_2 relative to the Al_2O_3 peaks are more intense with the Pd/BTiO_2-CM due to the higher coverage density of TiO_2 on the ceramic membrane after synthesis of branches. There are no obvious diffraction peaks of metallic Pd in the XRD patterns, which may be attributed to the low content and high dispersion of Pd nanoparticles.[32]

The FESEM observations provide the morphology of TiO_2 on the ceramic membrane. The surface FESEM image of Pd/TiO_2-CM is shown in Figure 3, from which it is evident that the surface of the TiO_2 nanorods is smooth and have diameters of 500- 1000 nm. Branched TiO_2 nanorods were synthesized successfully by treating the prepared TiO_2 nanorod-modified ceramic membranes in a titanium chloride solution at 80 °C. The morphology of the branched TiO_2 nanorods obtained after 16 hours of treatment is shown in the image of Pd/BTiO_2-CM.

This article is protected by copyright. All rights reserved.

The TiO_2 nanorods are fully covered by short needle-shaped branches which provide greater surface area (Table 1).

Pd nanoparticles in catalytic membranes

EDS mapping was performed on the three catalytic membranes to investigate the distribution of elemental Pd. In Figure 4, the red dots represent the Pd signal. Elemental Pd is present in a small amount on the surface of the Pd/CM, and the elemental Pd content significantly increases as a result of the modification of the TiO_2 nanorods and branched TiO_2 nanorods. The distribution of Pd on the surface of Pd/BTiO_2-CM is particularly dense and uniform, confirming that modification with branched TiO_2 nanorods can provide additional available surface for the loading of Pd nanoparticles. Furthermore, from the comparison of elemental Pd in sections of the three catalytic membranes, we can deduce that Pd nanoparticles are distributed in the pores of all three catalytic membranes. There are no obvious differences in the content of elemental Pd in the sections, since only a few TiO_2 nanorods and branched TiO_2 nanorods are synthesized in the pores. It may be that the small pore space (3 μm in mean pore size) prevents further synthesis of TiO_2 nanorods (approximately 3-5 μm in length) in the deeper membrane pores.

The Pd content of the three catalytic membranes was measured by ICP and the results are displayed in Table 1. The actual contents of Pd in Pd/CM, Pd/TiO_2-CM and Pd/BTiO_2-CM are 0.14, 0.19 and 0.37 mg/cm^2, respectively. The Pd/BTiO_2-CM has the

Accepted Article

This article is protected by copyright. All rights reserved.

highest Pd content, which is nearly three times greater than that found in the Pd/CM, and the trend is in good agreement with the EDS results (Figure 4). As expected, the total quantity of Pd in the reactor consisting of the Pd/BTiO$_2$-CM is the highest (3 mg). Therefore, we can deduce that modification with branched TiO$_2$ nanorods can effectively increase the surface area, resulting in increased loading amounts of Pd, which is one of the reasons for the improvement of catalytic activity.

Figures 5a-c show the distribution of Pd nanoparticles size in Pd/CM, Pd/TiO$_2$-CM and Pd/BTiO$_2$-CM. Taking into account of the errors of measurement, the average diameters of Pd nanoparticles in the three catalytic membranes are almost the same (about 4.2 nm). The HRTEM images of Pd nanoparticles (Figures 5d-f) show well-resolved lattice planes of Pd with a spacing of 0.22 nm corresponding to the (111) diffraction plane,[33] further confirming the successful loading of Pd nanoparticles. The lattice-spacing value of 0.32 nm in Pd/TiO$_2$-CM and Pd/BTiO$_2$-CM (Figures 5e and 5f) matches well with a (110) lattice plane of rutile TiO$_2$.[34] Furthermore, Figure 5g shows that Pd nanoparticles are immobilized on the trunks of the TiO$_2$ nanorods and TiO$_2$ branches, which could account for the higher Pd content in Pd/BTiO$_2$-CM (Figure 4 and Table 1).

Determination of pure water flux

When the temperature of water was 18 ^{o}C, the pure water flux values for the prepared catalytic membranes Pd/CM, Pd/TiO$_2$-CM and Pd/BTiO$_2$-CM are 16229, 9010 and 5883

Accepted Article

This article is protected by copyright. All rights reserved.

$L \cdot m^{-2} \cdot h^{-1} \cdot bar^{-1}$, respectively. The water flux drops sharply after synthesis of TiO_2 nanorods and branched TiO_2 nanorods on the ceramic membranes. Generally, the decrease in the membrane pore size will make the filtration resistance increase, thereby reducing the membrane flux.[35] In this work, the synthesis of TiO_2 nanorods and branched TiO_2 nanorods on the ceramic membranes makes the membrane pore size decrease (Table 1), leading to the reduced water flux. However, the water flux is still larger than the reported values. For example, the pure water flux reported by Mahdavi et al.[36] or Emin et al.[37] were 2-10 $L \cdot m^{-2} \cdot h^{-1} \cdot bar^{-1}$ and less than 1600 $L \cdot m^{-2} \cdot h^{-1} \cdot bar^{-1}$, respectively. The larger membrane pore size (approximately 3 μm) is responsible for the high water flux.

Evaluation of catalytic performance in a cycle mode

The PNP reduction process was evaluated in a cycle mode (Figure 6a). PNP reduction by Pd/CM converts approximately 36.8% of the PNP after 5 min, and its final reduction efficiency is 87.7% at 60 min. Under the same reaction conditions, Pd/TiO_2-CM exhibits a higher catalytic activity for PNP reduction (final conversion 95.4%). As expected, Pd/BTiO_2-CM achieves the highest reaction efficiency. The conversion of PNP over Pd/BTiO_2-CM increases from 57.2% at 5 min to 98.3% at 50 min, and the PNP pollutant can be reduced totally after 60 min. Figure 6b shows that the initial reaction rate during the first 5 minutes of the reaction using Pd/BTiO_2-CM is 1.6-fold higher than that using Pd/CM. The initial reaction rate in the system comprising Pd/TiO_2-CM is 1.1 times higher than that

Accepted Article

This article is protected by copyright. All rights reserved.

Accepted Article

comprising Pd/CM. These results illustrate that the branched TiO_2 nanorod arrays enhance the catalytic performance of Pd nanoparticles. The modification of ceramic membranes with branched TiO_2 nanorod arrays can provide additional surface area for the deposition of Pd nanoparticles, and thus higher Pd content can be obtained (Figure 4 and Table 1), resulting in enhanced catalytic performance. However, the increase of catalytic activity does not follow the increase of the Pd content, and the former is smaller than the latter. A possible explanation is that in Pd/TiO_2-CM and Pd/BTiO_2-CM, some Pd nanoparticles are immobilized between the TiO_2 nanorods or branched TiO_2 nanorods (Figure 5), and therefore some areas of the active Pd surface cannot be fully utilized.

The stability of catalytic membranes was evaluated by comparing the conversion of PNP in every recycling experiment. Once the reaction process was completed (60 minutes for each run), the catalytic membrane was removed and immersed in ethanol for 1 hour, then applied to the next reaction. As indicated in Figure 7, after 5 cycles of catalytic reduction of PNP using Pd/BTiO_2-CM, the conversion efficiency declined slightly but remained above 91.6%. For Pd/CM, after 5 cycles, the conversion efficiency of PNP was only 74.0%, which is significantly lower than that in the first run (87.7%). These results indicate that the branched TiO_2 nanorods are favorable for enhancing the catalytic stability of Pd nanoparticles. This may be because the TiO_2 branches can play a role in fixing Pd nanoparticles to prevent them from falling off during the recycling experiments (Figure 5). To assess this assumption, the

This article is protected by copyright. All rights reserved.

Accepted Article

Pd contents in Pd/CM and Pd/BTiO$_2$-CM were determined by ICP analysis after 5 recycling experiments. After 5 cycles, 27.4% of the Pd in Pd/CM was leached, and only 14.3% of the Pd in Pd/BTiO$_2$-CM was leached, thus confirming our assumption. However, the decline in the PNP conversion using Pd/CM and Pd/BTiO$_2$-CM were 15.6% and 8.4%, which are less than the leaching percentage of Pd. This observation may be related to the evolution of zero-valent Pd (Pd^0) in the catalytic membranes during the recycling experiments. To confirm this, the ratios of Pd^0 in Pd/BTiO$_2$-CM before and after 5 cycles were determined by XPS. As shown in Figure 8, after 5 cycles, the ratio of Pd^0 in Pd/BTiO$_2$-CM increased from 72% to 76%, which is likely due to the reduction of divalent Pd (Pd^{2+}) to Pd^0 by $NaBH_4$ during the reaction.[38] An increase in the Pd^0 can offset the negative effect of Pd leaching, leading to a lower decline of PNP conversion in comparison with the leaching percentage of Pd. In addition, Pd poisoning may be another reason for the catalyst deactivation, and the progressive replacement of poisoned catalyst by unused Pd could contribute to the observed constant activity. To obtain a catalytic membrane with better catalytic stability, based on our previous research,[26,30] the branched TiO_2 nanorod-modified ceramic membrane was modified further by AAPTS prior to loading of Pd nanoparticles, and the prepared catalytic membrane was designated as Pd/BTiO$_2$-CM-AAPTS. AAPTS has two functional groups: a hydroxyl (-OH) and an amine group (-NH_2) or imino group (-NH). The -OH can react with the -OH on the ceramic membrane via condensation and form strong -Si-O-Al- covalent bonds. The -NH_2

This article is protected by copyright. All rights reserved.

Accepted Article

or -NH is a strong electron donor and has a strong chelating ability for transition metals, thus the Pd can react with them to form a chelated complex and be bound to the ceramic membrane.[39] Therefore, AAPTS can promote the covalent bonding of Pd nanoparticles to the ceramic membrane. As expected, Pd/$BTiO_2$-CM-AAPTS can be reused 5 times with no decrease in the catalytic activity. ICP analysis was performed on the Pd/$BTiO_2$-CM-AAPTS after 5 recycling experiments. The result shows that the loading amount of Pd in the recovered Pd/$BTiO_2$-CM-AAPTS is almost the same as the fresh sample (0.37 mg/cm^2). These results indicate the good stability of Pd/$BTiO_2$-CM-AAPTS.

Evaluation of catalytic performance in a continuous mode

To investigate the feasibility of continuous conversion of PNP, a continuous operation mode was developed and the prepared Pd/$BTiO_2$-CM-AAPTS was evaluated.

To achieve the complete conversion of PNP, the dependence of PNP conversion on the residence time was first investigated. Figure 9 shows the degree of conversion when a 4.176 g/L solution of PNP flowed through the catalytic membrane in a continuous mode. The total amount of Pd in the two catalytic membranes in the reactor was 6 mg. A 99.4% conversion was achieved at 4 seconds of residence time (flux density 560 $L \cdot m^{-2} \cdot h^{-1}$). In accordance with the features of conventional flow-through reactors,[40] it is clear that an increasing residence time through the membrane results in an increase in the conversion of PNP, and the degree of conversion can reach 100% at 24 seconds of residence time (flux density 93 $L \cdot m^{-2} \cdot h^{-1}$). In

This article is protected by copyright. All rights reserved.

Accepted Article

addition, ICP analysis was performed on the permeate from the first membrane, and no Pd was found in the permeate, confirming the absence of Pd leaching. This result indicates that no leached Pd takes part in the reaction and only the catalytic membranes are responsible for the conversion of PNP. These results demonstrate the feasibility of attaining complete conversion of PNP in a flow-through membrane reactor in a continuous mode.

To evaluate the stability of the flow-through membrane reactor for the continuous complete conversion of PNP at a concentration of 4.176 g/L, the reduction process was performed under constant reaction conditions for 240 min. It can be seen clearly from Figure 10 that PNP conversion up to 100% can be achieved and that no deactivation occurs over a time period of 240 min. The images in Figure 10 show that the reaction solution changes from yellow to colorless after passing through the catalytic membrane reactor. The products collected in the reaction period of 220-240 min were analyzed by GC-MS. The GC-MS chromatogram (Figure 11) indicates that, except for the peaks of the ethanol (solvent), diethyl ether (extractant) and *p*-aminophenol, no other products were detected. Therefore, it can be concluded that the contaminant PNP can be continuously and thoroughly reduced to *p*-aminophenol within 240 min in a flow-through membrane reactor.

To evaluate the stability of Pd/BTiO_2-CM-AAPTS, TEM and ICP analyses were performed on the catalytic membranes before and after the continuous complete conversion of PNP. The average diameter of Pd nanoparticles in the recovered Pd/BTiO_2-CM-AAPTS

This article is protected by copyright. All rights reserved.

was not significantly different from the fresh particles and remained at 4.2 ± 0.2 nm (Figure 12). Based on the ICP analysis, the Pd content in the recovered Pd/BTiO$_2$-CM-AAPTS was 0.36 mg/cm^2, which is within the measurement error relative to the fresh one (0.37 mg/cm^2). These results further confirm the good stability of the flow-through membrane reactor for continuous conversion of PNP.

Insights into the enhancement mechanism of catalytic performance

The concentration of PNP used in our reaction is dozens or hundreds times higher than those reported in the literature, and the molar ratio of $NaBH_4$ to PNP is much smaller than literature values (Table 2). More importantly, Pd/BTiO$_2$-CM-AAPTS can achieve continuous complete conversion of PNP for more than 240 minutes, which has not been reported previously, especially at such a high concentration. In this work, the quantity of Pd used in the reactor is significantly higher than those reported in the literature (Table 2), and could account for the complete conversion of high concentrations of PNP with less consumption of $NaBH_4$. However, the $NaBH_4$ is still in a large excess (Table 2), far from the stoichiometric amounts required. $NaBH_4$ is easily hydrolyzed during the reaction, therefore excess $NaBH_4$ is often needed.[41] In future work, we will attempt to further reduce the amount of $NaBH_4$, enhance the catalytic efficiency of Pd and the stability of the catalytic membrane, and improve the economic efficiency of the catalytic membrane reactor. Notably, the productivity per g of catalyst in this work is almost the same as that in the work of Emin et al.[28]

Accepted Article

This article is protected by copyright. All rights reserved.

Accepted Article

irrespective of the different Pd contents, which may be caused by the flow-through mode.

The excellent catalytic activity of the catalytic membrane in this work may be attributed to the small size of the Pd nanoparticles, the higher quantity of Pd in the reactor, and the rapid mass transfer that is ascribed to the porous membrane structure and the flow-through mode. For example, in terms of particle size, the average size of Pd nanoparticles in the report of Wang et al.[24] was greater than 15 nm. A larger average diameter (approximately 26 nm) was found for the Pd nanoparticles in the PVDF composite membranes prepared by Xu et al.[42] However, the Pd nanoparticles in our research are only 4.2 ± 0.2 nm in size (Figure 12), which is much smaller than those reported in the literature and can provide more active sites for the conversion of PNP. Regarding the quantity of Pd used, the total amount of Pd in our reactor is 6 mg, which is significantly higher than those reported in the literature (Table 2). Furthermore, the flow-through catalytic membrane reactor is constructed with a porous membrane that is loaded with active Pd nanoparticles, and is operated in a dead-end mode to force the feed stream to flow over the active sites as shown in Figure 13. These features indicate that the reaction solution can more easily pass through the membrane and contact the active sites in the pores in our research, resulting in enhanced catalytic efficiency[23].

Conclusions

In summary, a novel flow-through catalytic membrane reactor system was designed and constructed for the continuous complete conversion of high concentration *p*-nitrophenol. The

This article is protected by copyright. All rights reserved.

modification of ceramic membranes with branched TiO_2 nanorods can enhance the Pd content but renders parts of the Pd nanoparticles unusable. High concentrations of *p*-nitrophenol can be completely converted with less consumption of $NaBH_4$ in a short time in the flow-through catalytic membrane reactor, which can be attributed to the small Pd nanoparticles, a higher Pd content and rapid mass transfer. The conversion efficiency remained at 100% for 240 minutes, and no byproducts were detected. The catalytic membrane reactor developed here provides a promising prospect for practical applications of industrial wastewater treatment.

Acknowledgments

The financial supports from the National Natural Science Foundation (21776127) and the Jiangsu Province Natural Science Foundation (BK20160978) of China are gratefully acknowledged. The work was also supported by the State Key Laboratory of Materials-Oriented Chemical Engineering (KL17-04).

Literature Cited

1. Rodrigues CSD, Soares OSGP, Pinho MT, Pereira MFR, Madeira LM. *p*-Nitrophenol degradation by heterogeneous Fenton's oxidation over activated carbon-based catalysts. *Appl. Catal. B: Environ.* 2017; 219: 109-122.
2. Mandlimath TR, Gopal B. Catalytic activity of first row transition metal oxides in the conversion of *p*-nitrophenol to *p*-aminophenol. *J. Mol. Catal. A: Chem.* 2011; 350: 9-15.

Accepted Article

This article is protected by copyright. All rights reserved.

Accepted Article

3. Bae S, Gim S, Kim H, Hanna K. Effect of $NaBH_4$ on properties of nanoscale zero-valent iron and its catalytic activity for reduction of *p*-nitrophenol. *Appl. Catal. B: Environ.* 2016; 182: 541-549.

4. Sun SP, Lemley AT. *p*-Nitrophenol degradation by a heterogeneous Fenton-like reaction on nano-magnetite: Process optimization, kinetics, and degradation pathways. *J. Mol. Catal. A: Chem.* 2011; 349: 71-79.

5. Mulchandani P, Hangarter CM, Lei Y, Chen W, Mulchandani A. Amperometric microbial biosensor for *p*-nitrophenol using *Moraxella* sp.-modified carbon paste electrode. *Biosens. Bioelectron.* 2005; 21: 523-527.

6. Chen HH, Yang M, Tao S, Chen GW. Oxygen vacancy enhanced catalytic activity of reduced Co_3O_4 towards *p*-nitrophenol reduction. *Appl. Catal. B: Environ.* 2017; 209: 648-656.

7. Lai B, Chen ZY, Zhou YX, Yang P, Wang JL, Chen ZQ. Removal of high concentration *p*-nitrophenol in aqueous solution by zero valent iron with ultrasonic irradiation (US-ZVI). *J. Hazard. Mater.* 2013; 250-251: 220-228.

8. Liu Y, Liu HL, Li Y. Comparative study of the electrocatalytic oxidation and mechanism of nitrophenols at Bi-doped lead dioxide anodes. *Appl. Catal. B: Environ.* 2008; 84: 297-302.

9. Pradhan AA, Gogate PR. Degradation of *p*-nitrophenol using acoustic cavitation and

This article is protected by copyright. All rights reserved.

Accepted Article

Fenton chemistry. *J. Hazard. Mater.* 2010; 173: 517-522.

10. Yi S, Zhuang WQ, Wu B, Tay STL, Tay JH. Biodegradation of *p*-nitrophenol by aerobic granules in a sequencing batch reactor. *Environ. Sci. Technol.* 2006; 40: 2396-2401.
11. Tomei MC, Annesini MC. 4-Nitrophenol biodegradation in a sequencing batch reactor operating with aerobic-anoxic cycles. *Environ. Sci. Technol.* 2005; 39: 5059-5065.
12. Bhatti ZI, Toda H, Furukawa K. *p*-Nitrophenol degradation by activated sludge attached on nonwovens. *Water Res.* 2002; 36: 1135-1142.
13. Shi XH, Zheng FC, Yan N, Chen QW. $CoMn_2O_4$ hierarchical microspheres with high catalytic activity towards *p*-nitrophenol reduction. *Dalton Trans.* 2014; 43: 13865-13873.
14. Zhong ZX, Xing WH, Jin WQ, Xu NP. Adhesion of nanosized nickel catalysts in the Nanocatalysis/UF System. *AIChE J*. 2007; 53: 1204-1210.
15. Wang AJ, Cheng HY, Liang B, Ren NQ, Cui D, Lin N, Kim BH, Rabaey K. Efficient reduction of nitrobenzene to aniline with a biocatalyzed cathode. *Environ. Sci. Technol.* 2011; 45: 10186-10193.
16. Shen JY, Xu XP, Jiang XB, Hua CX, Zhang LB, Sun XY, Li JS, Mu Y, Wang LJ. Coupling of a bioelectrochemical system for *p*-nitrophenol removal in an upflow anaerobic sludge blanket reactor. *Water Res.* 2014; 67: 11-18.
17. Lu H, Yin H, Liu Y, Jiang T, Yu L. Influence of support on catalytic activity of Ni catalysts in *p*-nitrophenol hydrogenation to *p*-aminophenol. *Catal. Commun.* 2008; 10:

This article is protected by copyright. All rights reserved.

Accepted Article

313-316.

18. Zhang WM, Zhou ZW, Shan XY, Xu R, Chen Q, He GY, Sun XQ, Chen HQ. Solvent-thermal preparation of a $CuCo_2O_4$/RGO heterocomposite: an efficient catalyst for the reduction of *p*-nitrophenol. *New J. Chem.* 2016; 40: 4769-4774.
19. Li H, Liao J, Zeng T. Application of Co/Ti film catalysts with different nanostructures in the reduction of *p*-nitrophenol to *p*-aminophenol. *Catal. Sci. Technol.* 2014; 4: 681-687.
20. Ding SS, Yan Q, Jiang H, Zhong ZX, Chen RZ, Xing WH. Fabrication of Pd@ZIF-8 catalysts with different Pd spatial distributions and their catalytic properties. *Chem. Eng. J.* 2016; 296: 146-153.
21. Huang RL, Zhu HX, Su RX, Qi W, He ZM. Catalytic membrane reactor immobilized with alloy nanoparticle-loaded protein fibrils for continuous reduction of 4-nitrophenol. *Environ. Sci. Technol.* 2016; 50: 11263-11273.
22. Strano MS, Foley HC. Synthesis and characterization of catalytic nanoporous carbon membranes. *AIChE J*. 2001; 41: 66-78.
23. Gu YY, Bacchin P, Lahitte J-F, Remigy J-C. Catalytic membrane reactor for Suzuki-Miyaura C-C cross-coupling: explanation for its high efficiency via modeling. *AIChE J*. 2017; 63: 698-704.
24. Wang Z, Chen X, Li K, Bi SY, Wu CL, Chen L. Preparation and catalytic property of PVDF composite membranewith polymeric spheres decorated by Pd nanoparticles in

This article is protected by copyright. All rights reserved.

membrane pores. *J. Membr. Sci.* 2015; 496: 95-107.

25. Domènech B, Muñoz M, Muraviev DN, Macanás J. Catalytic membranes with palladium nanoparticles: From tailored polymer to catalytic applications. *Catal. Today.* 2012; 193: 158-164.
26. Zhang S, Jiang H, Liu YF, Chen RZ. High catalytic efficiency of Pd nanoparticles immobilized on TiO_2 nanorods-coated ceramic membranes. *Can. J. Chem. Eng.* 2017; 95: 2374.
27. Macanás J, Ouyang L, Bruening ML, Munoz M, Remigy JC, Lahitte JF. Development of polymeric hollow fiber membranes containing catalytic metal nanoparticles. *Catal. Today.* 2010; 156: 181-186.
28. Emin C, Gu Y, Remigy JC, Lahitte JF. Polyethersulfone hollow fiber modified with poly(styrenesulfonate) and Pd nanoparticles for catalytic reaction. *Eur. Phys. J. Special Topics* 2015; 224: 1843-1848.
29. Eiden-Assmann S, Widoniak J, Maret G, Synthesis and characterization of porous and nonporous monodisperse colloidal TiO_2 particles. *Chem. Mater.* 2004; 16: 6-11.
30. Du Y. and Chen RZ. Fabrication of palladium nanoparticles immobilized on an amine-functionalized ceramic membrane support using a nanoparticulate colloidal impregnation method with enhanced catalytic properties. *Korean J. Chem. Eng.* 2015; 32: 1759-1765.

Accepted Article

This article is protected by copyright. All rights reserved.

Accepted Article

31. Huang H, Pan L, Lim CK, Gong H, Guo J, Tse MS, Tan OK. Hydrothermal growth of TiO_2 nanorod arrays and in situ conversion to nanotube arrays for highly efficient quantum dot-sensitized solar cells. *Small* 2014; 9: 3153-3160.

32. Zhong JB, Lu Y, Jiang WD, Meng QM, He XY, Li JZ, Chen YQ. Characterization and photocatalytic property of Pd/TiO_2, with the oxidation of gaseous benzene. *J. Hazard. Mater.* 2009; 168: 1632-1635.

33. Zhang Y, Liu C, Jiu B, Liu Y, Gong F. Facile synthesis of Pd-decorated ZnO nanoparticles for acetone sensors with enhanced performance. *Res Chem Intermed.* 2018; 44: 1569-1578.

34. Lv MQ, Zheng DJ, Ye MD, Sun L, Xiao J, Guo WX, Lin CJ. Densely aligned rutile TiO_2 nanorod arrays with high surface area for efficient dye-sensitized solar cells. *Nanoscale* 2012; 4: 5872-5879.

35. Zuriaga-Agustı´ E, Alventosa-deLara E, Barredo-Damas S, Alcaina-Miranda MI, Iborra-Clar MI, Mendoza-Roca JA. Performance of ceramic ultrafiltration membranes and fouling behavior of a dye-polysaccharide binary system. *Water Research* 2014; 54: 199-210.

36. Mahdavi H, Heidari AA. Chelated palladium nanoparticles on the surface of plasma-treated polyethersulfone membrane for an efficient catalytic reduction of *p*-nitrophenol. *Polym Adv Technol.* 2018; 29: 989-1001.

This article is protected by copyright. All rights reserved.

Accepted Article

37. Emin C, Remigy J-C, Lahitte J-F. Influence of UV grafting conditions and gel formation on the loading and stabilization of palladium nanoparticles in photografted polyethersulfone membrane for catalytic reactions. *J. Membr. Sci.* 2014; 455: 55-63.

38. Liu JC, He F, Durham E, Zhao D, Roberts CB. Polysugar-stabilized Pd nanoparticles exhibiting high catalytic activities for hydrodechlorination of environmentally deleterious trichloroethylene. *Langmuir* 2008; 24: 328-336.

39. Chen RZ, Jiang YG, Xing WH, Jin WQ. Fabrication and catalytic properties of palladium nanoparticles deposited on a silanized asymmetric ceramic support. *Ind. Eng. Chem. Res.* 2011; 50: 4405-4411.

40. Sakai S, Antoku K, Yamaguchi T, Kawakami K. Development of electrospun poly(vinyl alcohol) fibers immobilizing lipase highly activated by alkyl-silicate for flow-through reactors. *J. Membr. Sci.* 2008; 325: 454-459.

41. Sahiner N, Yildiz S, Al-Lohedan H. The resourcefulness of p(4-VP) cryogels as template for in situ nanoparticle preparation of various metals and their use in H_2 production, nitro compound reduction and dye degradation. *Appl. Catal. B: Environ.* 2015; 166-167: 145-154.

42. Xu LL, Ma SK, Chen X, Zhao C, Zhao YP, Chen L. A novel poly (vinylidene fluoride) composite membrane for catalysis and separation. *Polym. Eng. Sci.* 2017; 58: 150-159.

This article is protected by copyright. All rights reserved.

Accepted Article

Table 1. Specific surface area, pore size, Pd content and Pd quantity of three catalytic membranes

Samples	S_{BET} (m^2/g)	Pore size (μm)	Pd content (mg/cm^2)	Pd quantity in reactor (mg)
Pd/CM	0.16	4.3	0.14	1.1
Pd/TiO_2-CM	0.37	3.3	0.19	1.5
Pd/BTiO_2-CM	1.45	2.9	0.37	3

This article is protected by copyright. All rights reserved.

Accepted Article

Table 2. Comparison of PNP conversion by catalytic membranes.

Samples	PNP concentration (ppm)	Flux density ($L \cdot m^{-2} \cdot h^{-1}$)	$NaBH_4$:PNP molar ratio	Operation mode	Pd quantity in reactor (mg)	Reaction temperature (^oC)	Reaction time (s)	Conversion (%)	References
PVDF/PMAA-Pd	20	-	2469	cross-flow	-	20	-	95	Xu et al. [42]
Pd/PVDF	20	-	419	cross-flow	-	25	1200	99.8	Wang et al. [24]
Pd/SPES-C	70	-	100	batch reactor	-	-	18000	90	Domènech et al. [25]
PES-PSS5/Pd	100	55	100	flow through	0.086	-	1.3	100	Emin et al. [28]
PY-300-PES	100	-	20	penetration	2.4	-	1740	100	Mahdavi et al. [36]
PSS-PAA8	100	30	20	flow through	0.33	RT	0.15	90	Emin et al. [37]
Pd/BTiO_2-CM-AAPTS	**4176**	**93**	**9.6**	**flow through**	**6**	**30**	**24**	**100**	**In this work**

This article is protected by copyright. All rights reserved.

Accepted Article

Figure Captions

Figure 1. Experimental setup of a flow-through catalytic membrane reactor.

Figure 2. XRD patterns of three catalytic membranes.

Figure 3. Surface FESEM images of three catalytic membranes.

Figure 4. EDS analysis of the distribution of elemental Pd on three catalytic membranes.

Figure 5. TEM images of (a, d) Pd/CM, (b, e) Pd/TiO_2-CM and (c, f, g) Pd/$BTiO_2$-CM.

Figure 6. (a) Reduction efficiency for 4.176 g/L PNP by Pd/CM, Pd/TiO_2-CM and Pd/$BTiO_2$-CM, (b) Initial reaction rate using three catalytic membranes. (Reaction conditions: temperature, 30 ^oC; PNP concentration, 4176 mg/L; molar ratio of $NaBH_4$/PNP, 9.6; Pd quantity in the reactor: (Pd/CM), 1.1 mg; (Pd/TiO_2-CM), 1.5 mg; (Pd/$BTiO_2$-CM), 3.0 mg)

Figure 7. Correlation of the conversion with repeated runs. (Reaction conditions: temperature, 30 ^oC; PNP concentration, 4176 mg/L; molar ratio of $NaBH_4$/PNP, 9.6; reaction time for each run, 60 minutes; Pd quantity in the reactor: (Pd/CM), 1.1 mg; (Pd/$BTiO_2$-CM), 3.0 mg; (Pd/$BTiO_2$-CM-AAPTS), 3.0 mg)

Figure 8. Pd 3d XPS spectra of (a) fresh Pd/$BTiO_2$-CM and (b) Pd/$BTiO_2$-CM after 5 cycles.

Figure 9. Effect of residence time on PNP conversion by a catalytic membrane reactor in a continuous operation mode. (Reaction conditions: temperature, 30 ^oC; PNP concentration, 4176 mg/L; molar ratio of $NaBH_4$/PNP, 9.6; Pd quantity in the reactor, 6 mg)

Figure 10. Stability of continuous flow-through membrane reactor for PNP reduction. (Reaction conditions: temperature, 30 ^oC; PNP concentration, 4176 mg/L; molar ratio of $NaBH_4$/PNP, 9.6; residence time, 24 seconds; Pd quantity in the reactor, 6 mg)

This article is protected by copyright. All rights reserved.

Figure 11. GC-MS analysis of the products collected in the reaction period of 220-240 min from the continuous flow-through membrane reactor.

Figure 12. TEM images of Pd/BTiO$_2$-CM-AAPTS before (a) and after (b) continuous reaction.

Figure 13. Conversion of PNP to *p*-aminophenol in a flow-through catalytic membrane.

Accepted Article

This article is protected by copyright. All rights reserved.

Accepted Article

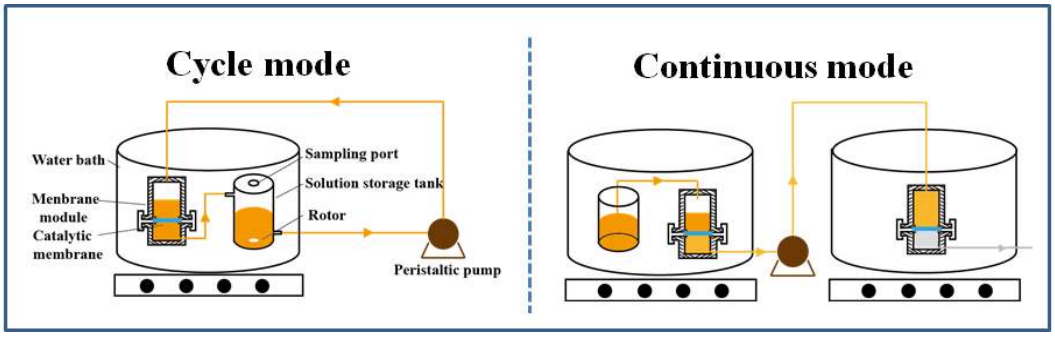

Figure 1

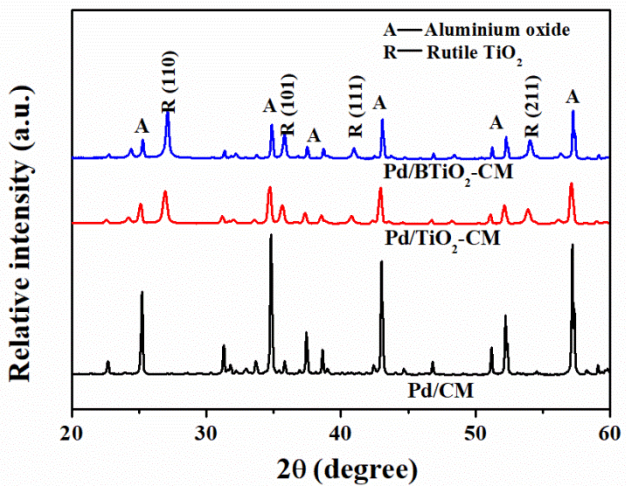

Figure 2

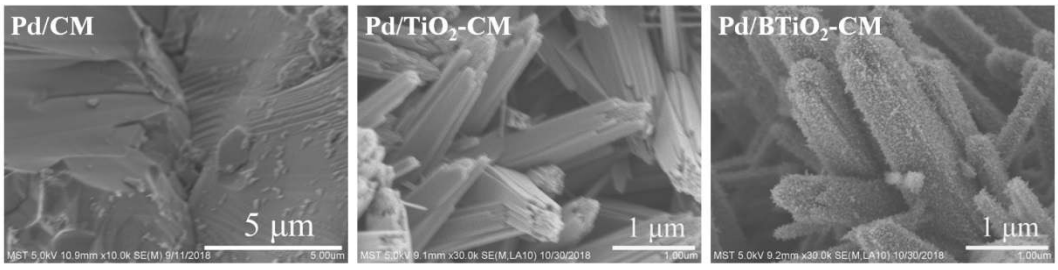

Figure 3

This article is protected by copyright. All rights reserved.

Accepted Article

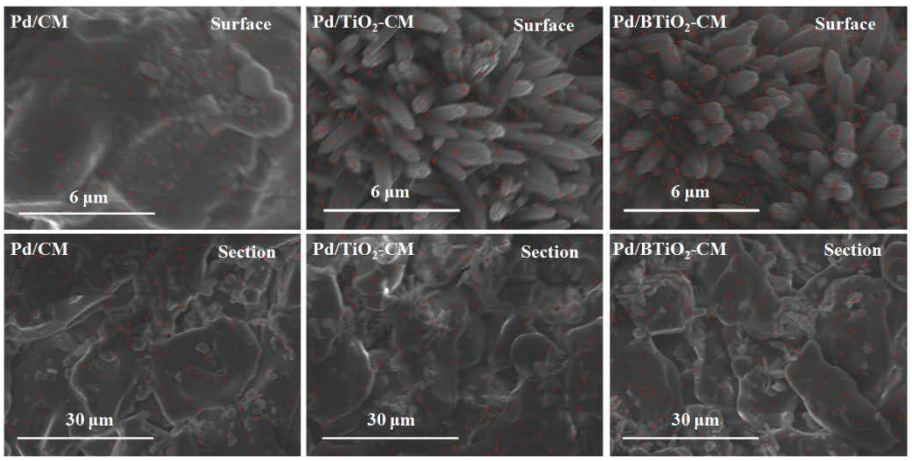

Figure 4

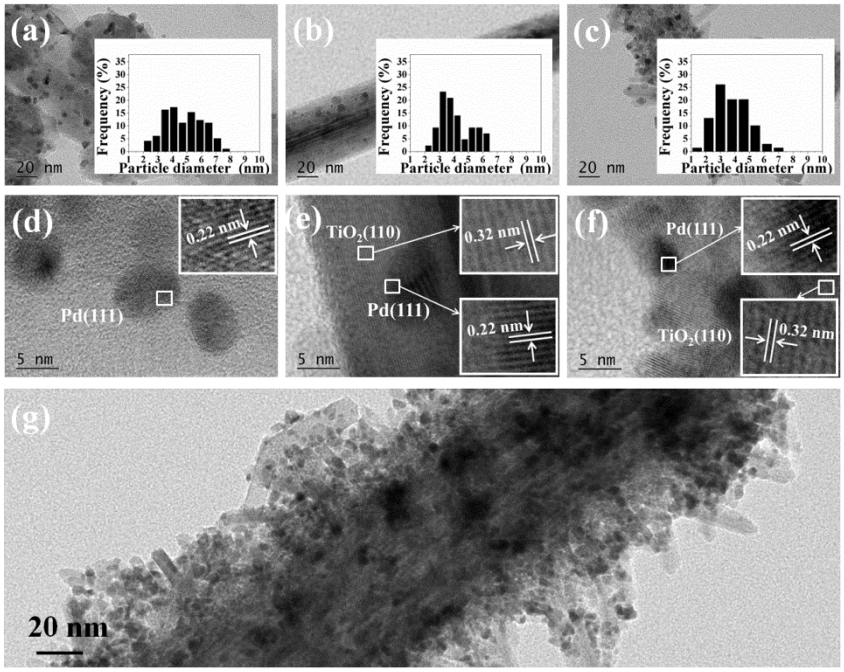

Figure 5

This article is protected by copyright. All rights reserved.

Accepted Article

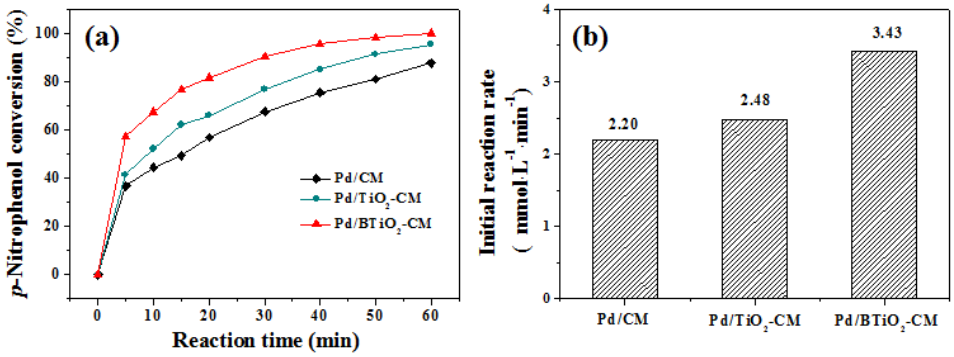

Figure 6

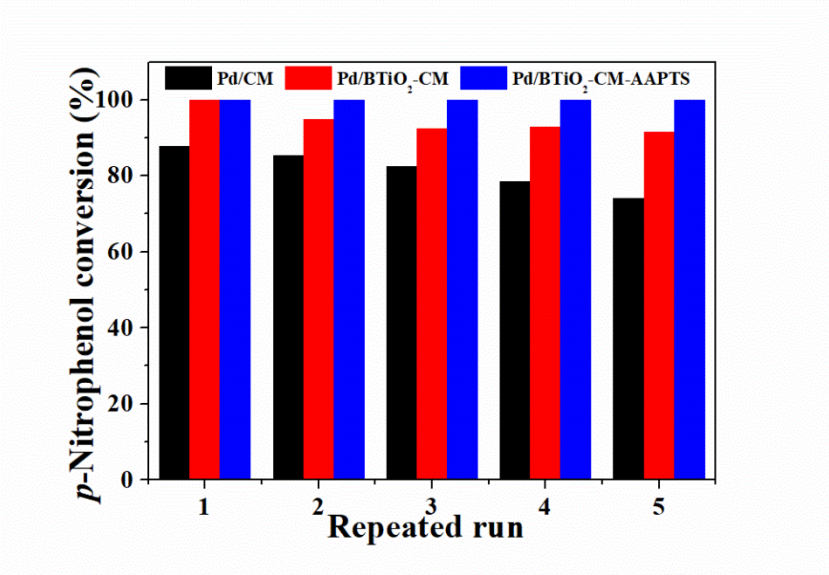

Figure 7

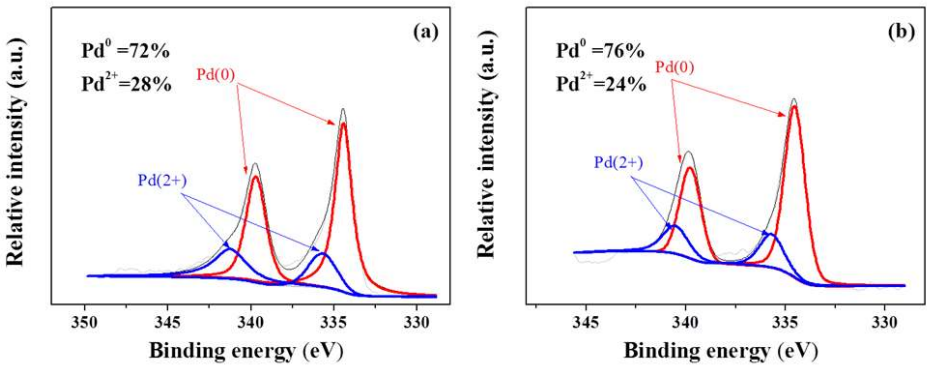

Figure 8

This article is protected by copyright. All rights reserved.

Accepted Article

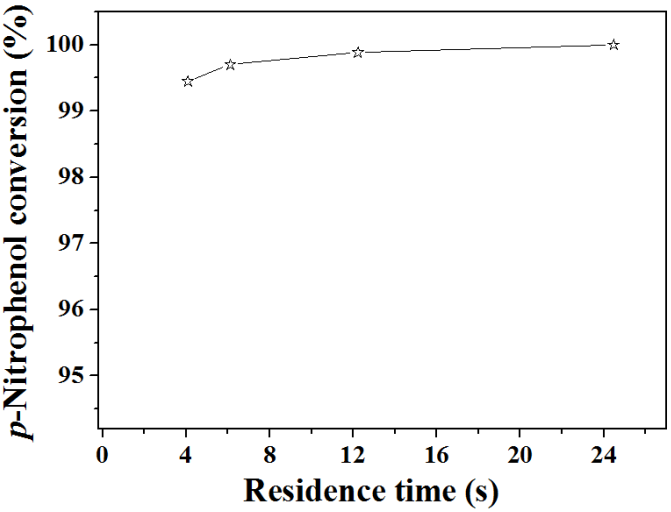

Figure 9

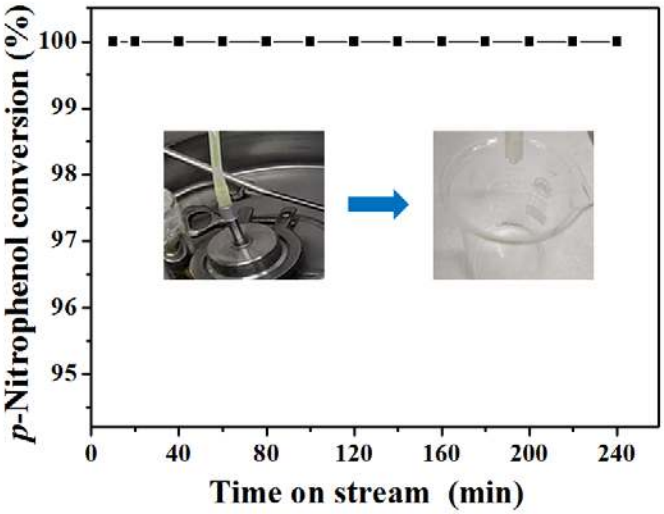

Figure 10

This article is protected by copyright. All rights reserved.

Accepted Article

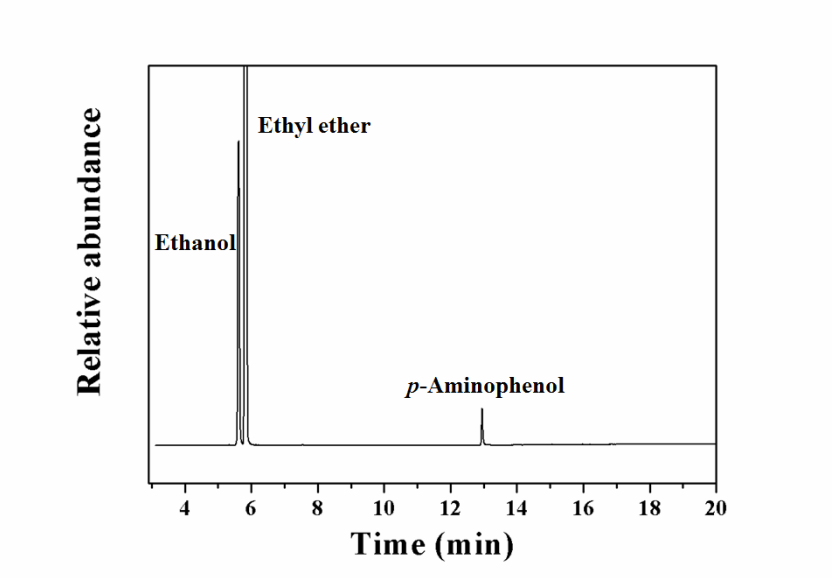

Figure 11

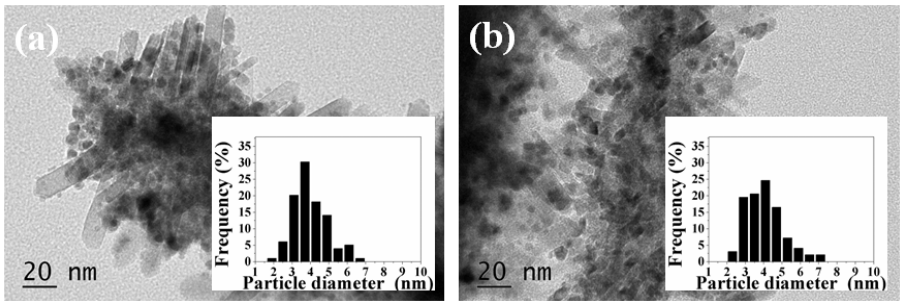

Figure 12

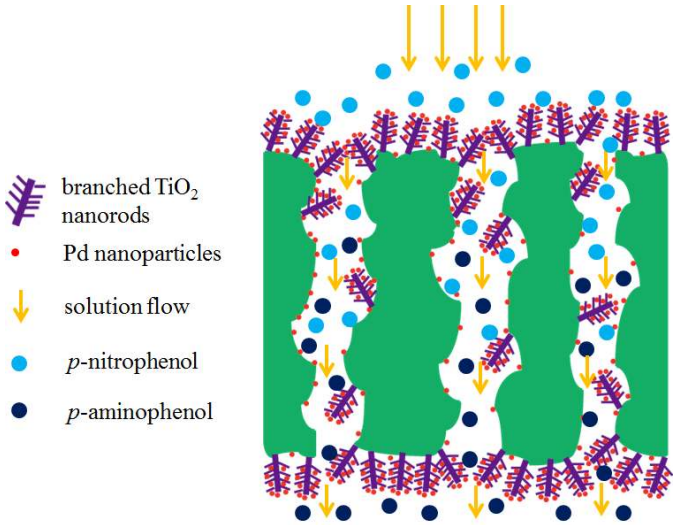

Figure 13

This article is protected by copyright. All rights reserved.